LiB and its boron-deficient variants under pressure

Andreas Hermann,[1,*] Ainhoa Suarez-Alcubilla,[2,4] Idoia G. Gurtubay,[2,3] Li-Ming Yang,[3] Aitor Bergara,[2,3,4]
N. W. Ashcroft,[5] and Roald Hoffmann[1]

[1]*Department of Chemistry and Chemical Biology, Cornell University, Ithaca, NY 14853, USA*

[2]*Materia Kondentsatuaren Fisika Saila, Zientzia eta Teknologia Fakultatea, Euskal Herriko Unibertsitatea, UPV/EHU,
644 Postakutxatila, 48080 Bilbo, Basque Country, Spain*

[3]*Donostia International Physics Center (DIPC), Paseo de Manuel Lardizabal, 20018, Donostia, Basque Country, Spain*

[4]*Centro de Fisica de Materiales CSIC-UPV/EHU, 1072 Posta kutxatila, E-20080 Donostia, Basque Country, Spain*

[5]*Laboratory of Atomic and Solid State Physics, Cornell University, Ithaca, NY 14853, USA*

Results of computational investigations of the structural and electronic properties of the ground states of binary compounds LiB_x with $0.67 \leqslant x \leqslant 1.00$ under pressure are reported. Structure predictions based on evolutionary algorithms and particle swarm optimization reveal that with increasing pressure, stoichiometric 1:1-LiB undergoes a variety of phase transitions, is significantly stabilized with respect to the elements and takes up a diamondoid boron network at high pressures. The Zintl picture is very useful in understanding the evolution of structures with pressure. The experimentally seen finite range of stability for LiB_x phases with $0.8 \leqslant x \leqslant 1.00$ is modeled both by boron-deficient variants of the 1:1-LiB structure and lithium-enriched intercalation structures. We find that the finite stability range vanishes at pressures $P \geqslant 40$ GPa, where stoichiometric compounds then become more stable. A metal-to-insulator transition for LiB is predicted at $P = 70$ GPa.

I. INTRODUCTION

Two of the lightest elements, lithium and boron, and their compounds, are very much a focus of high-pressure studies today. Each element by itself has special features; lithium seems to be a "simple" metal, yet it undergoes a series of structural changes as the pressure is raised, with complex structures that deviate from simple close-packed atomic arrangements at pressures of 30–40 GPa and higher.[1–3] Under these conditions, the "simple" element seems to enter the liquid regime below room temperature, and also shows a metal-insulator-metal transition.[3–5] Boron, close to the metal-nonmetal line, presents us with a set of complex structures from the outset, these characterized by electron-deficient bonding with icosahedral units.[6,7] At higher pressures, the structural complexity persists, as various other complex crystal structures are taken up by boron.[8–14]

In the Li/B phase diagram at $P = 1$ atm, one finds LiB, LiB_3, Li_3B_{14}, and a poorly characterized LiB_7 phase.[15,16] In a separate study, some of us have examined this phase diagram in some detail, and over a range of stoichiometries and pressures.[17] Here, we concentrate on the 1:1 LiB compound and some stoichiometries near to it. The reason for going off stoichiometry will become clear once we describe the structure, but is related to the fact that the experimental stability range of this phase actually exceeds the 1:1 ratio on the lithium-rich side: it is stable up to about 55% lithium atomic content, or a 11:9 ratio of Li:B. As we will see, a further reason for interest in 1:1 LiB is that at high pressures, this phase dominates the convex hull for the binary phase diagram.

II. METHODOLOGY

We began our exploration by looking at the experimentally known LiB structure. We also tried static structures for LiB (and also boron-deficient versions) based on known A_xE_y phase structures, where A and E are heavier elements from groups 1 and 13, respectively. And we explored possible phases with structures searches based on evolutionary algorithms[18–20] and the particle swarm optimization method.[21,22] Density functional theory as implemented in the VASP package (version 5.2) was used to evaluate total energies and enthalpies of the phases,[23–25] employing the projector augmented wave dual-basis approach[26,27] and the PBE parameterization of the exchange-correlation functional.[28] A plane-wave cutoff energy of at least $E_c = 400$ eV was used, the Brillouin zones were sampled with regular k-point meshes[29] with a linear density of $40/\text{Å}^{-1}$ ($80/\text{Å}^{-1}$ for DOS calculations), and structures were optimized until remaining forces on the atoms were below 1 meV/Å, or total energy changes that were less than 0.1 meV/atom. All enthalpies discussed in this work are for the ground state, enthalpy corrections from dynamical effects are not included. Crystal structures of the various phases can be found in Supplemental Material to this article[30] (see also references therein [31]).

III. LiB: LOW AND MEDIUM PRESSURE STRUCTURES

The 1:1 phase LiB has been found in experiment to take up a hexagonal crystal structure, space group 194, $P6_3/mmc$.[32,33] The primitive unit cell contains two boron and two lithium atoms each, which were assigned to Wyckoff sites *2b* and *2c*, respectively.[32] There are several alternative ways to see this structure, namely, (i) a simple hexagonal lithium lattice with linear boron chains in the cavities along the c axis, (ii) stacked hexagonal sheets of boron atoms with lithium in interstitial sites, or (iii) as staggered stacks of graphitic LiB sheets. Two of these views are presented in Fig. 1. The first one (of boron chains in a lithium network) is possibly most suggestive, for experiment indicates that the positions of the boron atoms along the c axis are uncorrelated,[33] which was explained by the small barriers needed to move
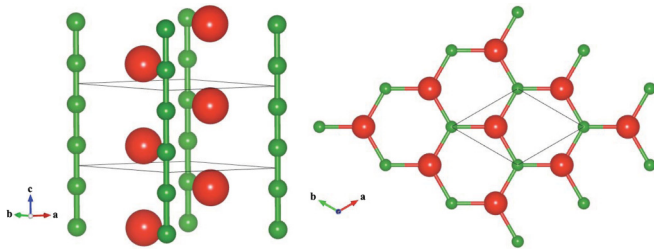
FIG. 1. (Color online) LiB crystal structure, as proposed by Liu *et al.*[32] The unit cell is indicated, and big red/dark gray (small green/light gray) spheres denote Li (B) atoms. (Left) Side view, emphasizing boron chains. (Right) Top view, emphasizing mixed Li-B graphitic sheets.

the boron chains against the lithium sublattice.[34] A more recent low-temperature neutron diffraction experiment of the "LiB" phase confirmed a synthesis product with stoichiometry $LiB_{0.885}$ and found that the lithium and boron sublattices are incommensurate, and that the disordered boron chains became ordered relative to each other as the temperatures decreased down to $T = 2$ K.[35] An even more recent experimental high-pressure x-ray diffraction study of "LiB" performed at room temperature estimated the initial composition to be $LiB_{0.92}$.[36] There seems to be agreement in those more recent experimental studies that the initial assignment of the stoichiometry 1:1 to "LiB" [32] might have been too optimistic.

A computational study of the system by Kolmogorov and Curtarolo [37] used the viewpoint of boron chains to investigate the stability of LiB_x compounds with $0.8 \leqslant x \leqslant 1$. By slightly decreasing the density of boron atoms within the chains (in an appropriate commensurate supercell), various compositions of LiB_x were constructed and shown to be more stable than pure LiB, at atmospheric and moderate pressures (up to $P = 30$ GPa).

For stoichiometric LiB, the B-B distance in the experimental structure is 1.40 Å. If one electron is transferred from Li to B, the B^- chain is then isoelectronic to C. A carbon allotrope of such chains has been persistently claimed in the literature, often called *karbin* or *carbyne*.[38–40] The structure of an infinite C_n chain might be a cumulene (all C-C double bonds) or have alternating single and triple bonds. Either way, the average C-C distance (therefore the average B-B distance in an isoelectronic poly-B^-) should be short. Can we estimate how short? A B-B triple bond in a molecule is around 1.56 Å[41] and a B-B single bond around 1.70 Å. Hence a comfortable B-B distance in a cumulene or alternating triply/singly bonded B-chain should be around 1.63 Å; this is in fact significantly longer than what is found in the experimental structure. This
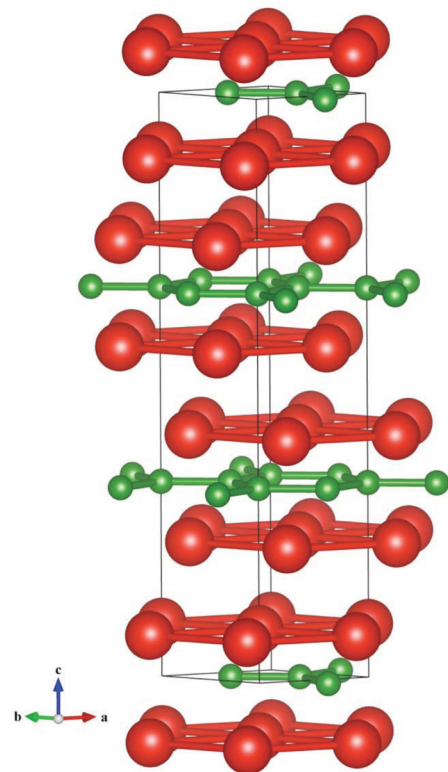

FIG. 2. (Color online) The *R-3m* "metal sandwich" structure of LiB, shown at $P = 1$ atm in the hexagonal unit cell.

point is not original, it was obvious to some of the structural chemists investigating this phase.[35]

The structural properties of stoichiometric LiB from our calculations are compared to experimental data and other theoretical results in Table I. In accord with other density functional studies,[34,37] we find very good agreement for the in-plane lattice constant a, but an overestimation of the c/a ratio of the unit cell by about 10%. The latter is not improved by choosing a different exchange-correlation functional,[42] including screened exact exchange,[43,44] or including dispersion effects at a semi-empirical level.[45] The increased c/a ratio leads to B-B distances of 1.56 Å, much longer than the 1.40 Å found in experiment; but much closer to what should be a chemically comfortable B-B distance.

However, and in agreement with other theoretical studies, we find that the experimentally proposed structure is actually not the ground state structure for 1:1-LiB at $P = 1$ atm:[46,47] an evolutionary and particle swarm optimization structure search at $P = 1$ atm (with $Z = 2$ formula units per unit cell) resulted in a more stable structure with *R-3m* symmetry at

TABLE I. Calculated lattice parameters for hexagonal LiB, compared to experiment and other theoretical results.

	Exp.[32]	This work, different XC functionals					Ref. 34	Ref. 37
		PBE	LDA	PW91	HSE06	PBE + D2	LDA	PBE
a (Å)	4.022	4.023	4.028	4.028	4.026	3.909	4.019	4.013
c (Å)	2.796	3.111	3.111	3.106	3.096	3.065	3.102	3.120
c/a	0.695	0.77	0.77	0.77	0.77	0.78	0.77	0.78

low to medium pressures, as shown in Fig. 2. This geometry, called a "metal sandwich" structure in Ref. 46, is comprised of graphitic layers of B atoms, sandwiched between trigonal nets of Li atoms. Its synthesis has been attempted.[36] We find this *R-3m* structure to be more stable than the experimental *P6₃/mmc* structure by about 5 meV per formula unit at $P = 1$ atm; however, as we shall see below, the *R-3m* structure is also unstable with respect to nonstoichiometric LiB_x structures with less dense boron chains than the 1:1 *P6₃/mmc* structure.

At 0 GPa, we also found another ground state *P6₃/mmc* structure, characterized by lattice constants $a = 3.988$ Å and $c = 3.138$ Å with Li at *2c* and B at *2a* Wyckoff positions, which is even more stable (around 20 meV per formula unit) than the room temperature experimental and the *R-3m* structure. This structure is typically referred to as *β*-LiB, and consists of hexagonal sheets of B with Li lying at alternating interstitial sites along the *c* axis and shifted relative to the B hexagonal planes along the *c* axis by $c/4$. This is the main difference with respect to the *α*-LiB structure, where Li and B atoms are located within the same planes. Interestingly, when the *β*-LiB structure is relaxed above 40 GPa it transforms to the diamond-like *Fd-3m* structure, which becomes the favored one above 70 GPa (see below).

The energy cost involved in laterally shifting adjacent Li-B-Li "sandwiches" is very small, and a resulting manifold of lower-symmetry *C2/m* structures could also be accessible to experiment. We probed this by rigidly shifting one Li-B-Li sandwich layer in the hexagonal basal plane along the *a* axis (the hexagonal unit cell has three of these layers), while keeping the other atoms fixed. Starting from the optimized structure at atmospheric pressure, a translation by a full unit cell has an energy barrier of only 0.25 eV. Similarly, pulling the Li-B-Li layers apart costs little energy: starting from the optimized structure at atmospheric pressure, increasing the distance between adjacent boron layers to infinity (while optimizing the positions of the Li atoms, which keep the Li-B-Li sandwich intact), costs only 0.2 eV per sandwich layer.

IV. LiB: DIAMONDOID NETS AT HIGH PRESSURES

At higher pressure ($P \geqslant 70$ GPa), we find that the ground state *R-3m* structure becomes itself unstable with respect to the NaTl structure, which is also found in LiAl,[48] and that the CsCl structure type also becomes more stable than the experimental LiB structure at high pressures. The latter structure is also found in LiTl.[49] Figure 3 shows the relative enthalpy curves for the various structures, the reference being the *P6₃/mmc* structure of *α*-LiB. We find a predicted phase transition for LiB at low pressures to *R-3m*, and at about $P = 70$ GPa to *Fd-3m*, the NaTl structure. Other structures we found in our structure search at $P = 1$ atm, of *Imma*, *Cmcm*, and *Cmmm* symmetry, are not competitive at high pressures. The NaTl structure is significantly stabilized over these and the experimentally known structure (note the energy scale in Fig. 3), which leads to the stability of the LiB phase in the Li-B phase diagram up to very high pressures.
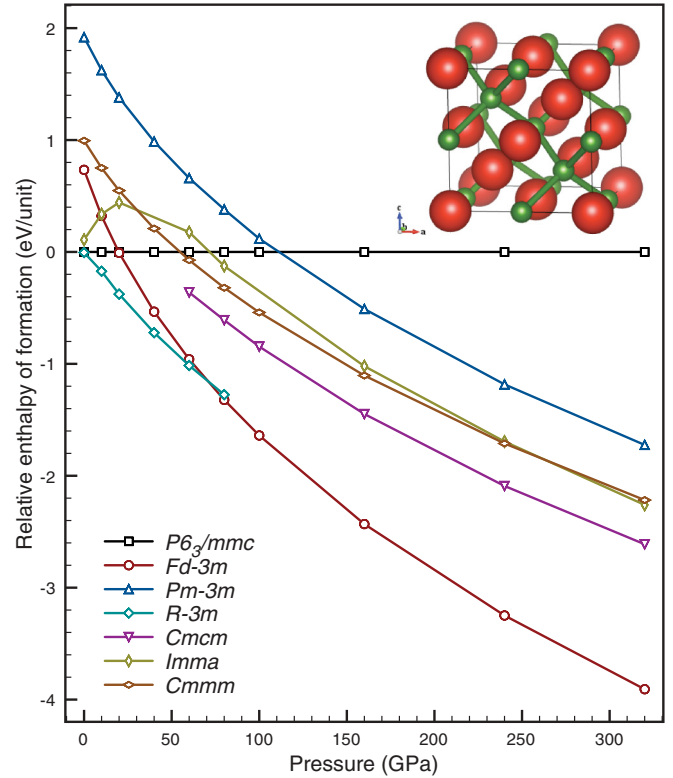

FIG. 3. (Color online) Relative enthalpies of formation of various LiB phases in the ground state. Inset shows the NaTl structure type for LiB, structure optimized at $P = 80$ GPa.

V. ZINTL VIEWPOINT AND ELECTRONIC STRUCTURE

A very useful concept in understanding compounds of electropositive metals (such as the alkalis or alkaline earths) and electronegative main group elements is the Zintl-Klemm formalism:[50–52] formally, the electropositive constituent transfers its electrons to the electronegative partner, which in turn forms a covalently bonded sublattice that corresponds to an element isoelectronic to the anion. For instance, anions Si^{2-} or P^- would be expected to form chain structures typically found in sulphur. While the metal cations do not retain any valence electrons, the anions, if bonded in a covalent network, can formally fulfill the electronic octet. Often, this leads to insulating phases. The prototypical Zintl phase, NaTl (where the Tl^- anions form a diamond lattice with Na^+ cations in tetrahedral holes) is, however, an exception to this rule (as far as metallicity goes; structurally, it fits), as it is found to be metallic.[53]

The utility of Zintl-type reasoning emerges in the high-pressure region of the phase diagram. If B^- is viewed as isoelectronic to C, it makes sense that (B^-) chains would quickly give way to more dense graphitic structures, which in turn would be unstable with increasing pressure to still denser diamondoid structures, with Li^+ in the interstices, forming a second diamondlike net. In the carbon phase diagram, diamond is stabilized over graphite at relatively low pressures, around 1.4 GPa at low temperatures.[54]

Electronically, both the experimental (*P6₃/mmc*) and theoretical (*R-3m*) ground-state structures at low pressure are metallic. The electronic density of states (DOS) for the
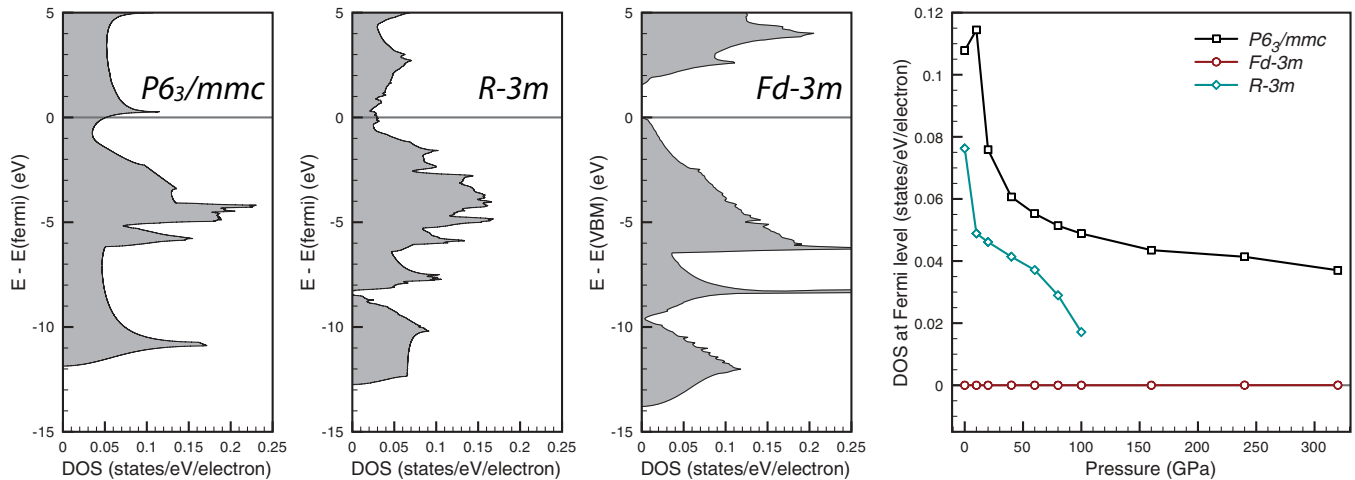
FIG. 4. (Color online) Electronic DOS of various ground states LiB phases, all at $P = 80$ GPa. From left: $P6_3/mmc$, R-$3m$, and Fd-$3m$ structures. The evolution of the DOS at the Fermi level with increased pressure is shown on the right.

experimental $P6_3/mmc$ structure exhibits the typical peak-like onset associated with a one-dimensional electron gas, see Fig. 4. In contrast, the R-$3m$ structure shows the square onset at low energies that is seen in two-dimensional electronic systems (see Fig. 4 as well). Both these characteristics corroborate the structural interpretations given above, with individual boron chains and sheets in the respective structures. The high-pressure Fd-$3m$ structure is, however, a semiconductor, at all pressures studied. This supports the Zintl interpretation of the structure of this phase. As it is the case for highly compressed lithium and sodium,[5,55–57] electronic states in LiB become increasingly localized with pressure and, above 70 GPa, present a metal-insulator transition, which persists up to at least 320 GPa, or a volume compression of $V_0/V = 6.25$ (where V_0 is the calculated volume for LiB in the $P6_3/mmc$ structure at $P = 1$ atm).

The band structures add some further insight into the electronic structure of these phases: note the low-energy bands in the $P6_3/mmc$ structure, with little dispersion within the hexagonal plane, but very strong dispersion along the hexagonal c axis (see Fig. 5). The metallicity in the R-$3m$ structure stems from a small band overlap, and looking at the depletion of the DOS at the Fermi level, this overlap seems to decrease with increased pressure. We intend to analyze the evolution of a possible superconducting phase and its superconducting T_c with pressure in this MgB$_2$-like structure. It has been shown that pressure increases the electronic localization and, therefore, decreases the electronic screening, which might enhance the electron-ion interaction and, accordingly, the associated superconducting transition temperature, as is the case in many other elements and compounds.[58]

VI. GOING OFF 1:1 STOICHIOMETRY WITH B-DEPLETED CHAINS

The finite stability range for the LiB phase (extending towards a maximum lithium content of about 55%) is
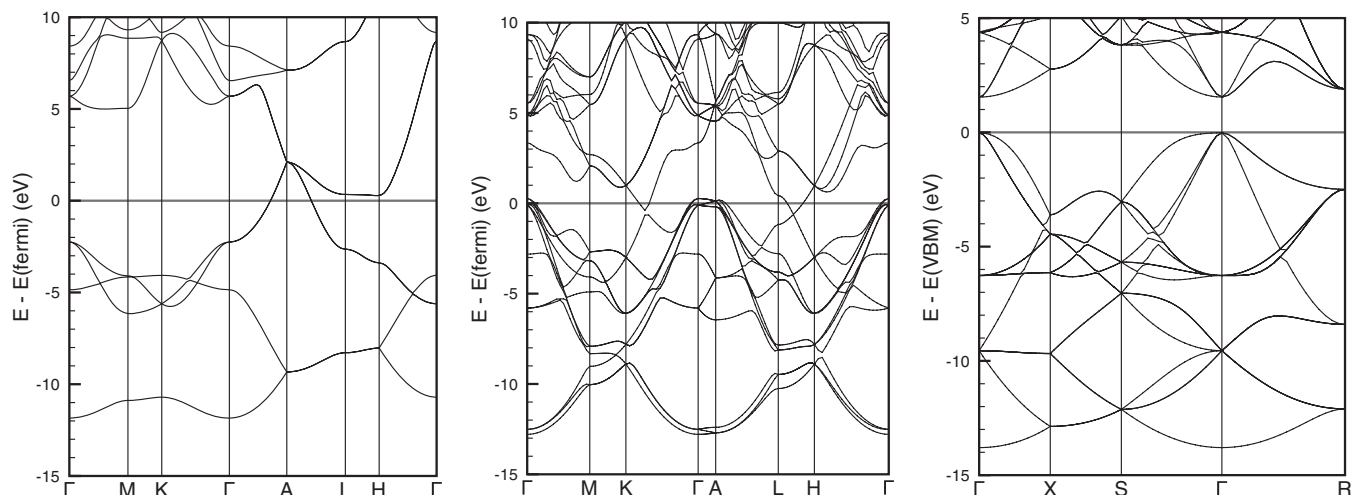

FIG. 5. Electronic band structures for various LiB phases. From left to right: $P6_3/mmc$, R-$3m$, and Fd-$3m$ structures, all at $P = 80$ GPa. The hexagonal unit cell for R-$3m$ and the conventional unit cell for the Fd-$3m$ structure were used.

puzzling. In light of the very different structural models for stoichiometric LiB proposed above, there are two ways to think about this: either by creating *boron deficient* LiB_x structures ($x < 1$, starting from the boron chain structure found in experiment[32,33,35]), or by creating *lithium enriched* Li_yB structures ($y > 1$, but now starting from the metal sandwich structures [46]).

Regarding the first of these options, we and others [35,37,46] noted that the 1:1 LiB $P6_3/mmc$ structure has B-B separations along the chain that are very short. The implication is that some loss of boron from the structures might have a stabilizing effect. We began an exploration of slightly boron deficient compounds by removing just 1 B atom for every 10 Li, to get $Li_{10}B_9$, for which we have then performed a particle swarm optimization structure search at $P = 1$ atm, with one formula unit per unit cell. At this pressure the best ground-state structural candidate is a hexagonal structure, space group 187, *P-6m2*, which is clearly favored (more than 100 meV/atom lower in energy) with respect to the next competitive phase. This structure can also be derived from α-LiB or β-LiB in the 1:1 stoichiometry, when every tenth B atom along the chain is removed and all the atoms are allowed to relax to their equilibrium positions. Note that although the boron concentration is lower in $Li_{10}B_9$, the B-B distance along the chains ($d = 1.56$ Å) remains almost unchanged compared to LiB, as the removal of B atoms from the α-LiB or β-LiB structures induces a strong contraction of the c axis. In fact, the c/a ratio for $Li_{10}B_9$ (considering only the hexagonal lithium sublattice's unit cell) is 0.71, in good agreement with experimental results for "LiB" ($c/a = 0.695$, see Ref. [32]), $LiB_{0.885}$ (0.696, see Ref. [35]), and $LiB_{0.92}$ (0.718, see Ref. [36]). The same structure was suggested by others.[35,37]

We went ahead further and created other boron-deficient chain structures Li_mB_n with $n < m$, using $n = 10$ and 12 supercells for the lithium sublattice. The quadratic dependency of the binding energy on the lithium content found in an earlier computational study was confirmed, and our predicted optimal atomic lithium content of 52.9% at atmospheric pressure

is in very good agreement with this study and the (room temperature) experimental result of 53.1%.[35,37]

Under pressure, the various chain structures become more stable with respect to the elements, see Fig. 6. However, the optimal lithium content increases (up to 58.7% at $P = 60$ GPa); this corresponds to an optimal $x = 0.70$ in LiB_x. The reason for this drastic change towards more boron-deficient stoichiometries under pressure can be deduced from perusal of the components of the respective enthalpies, the internal energies E and the volume-pressure term $p*V$, which are both shown in Fig. 6 as well. The minimum of the internal energy curve (vs. lithium content) does not change much under pressure. In contrast, the $p*V$ term clearly drives the enthalpy minimum towards the more boron-deficient structures. This is because the volume per atom decreases monotonously with increased lithium content, at all pressures.

Put another way, the unit cell volume is to a large degree determined by the boron sublattice, which fixes the hexagonal c axis (optimized B-B distances vary little when the composition is changed); the fewer boron atoms per lithium are available, the shorter the c axis will be, and thus the more the lithium sublattice is compressed. At atmospheric pressure and room temperature, there is an optimal atomic ratio that balances the needs of the two sublattices; at higher pressures, the more boron-deficient structures, which are more densely packed, are favored. In other studies, this was also explained from an electronic point of view, with the Fermi energy at the optimal composition being located in a pseudogap;[37] we find this not to be the case under pressure (see Supplemental Material[30] for details). Incidentally, we find the more boron-deficient structures to be less compressible: reducing the amount of the stronger bonding element (boron) leads to a stiffer compound (see Ref. [30] for details). That is because in a compound with two distinct sublattices, properties such as compressibility are determined by the *weaker* bonding element (here lithium), which is more precompressed if less boron is included.
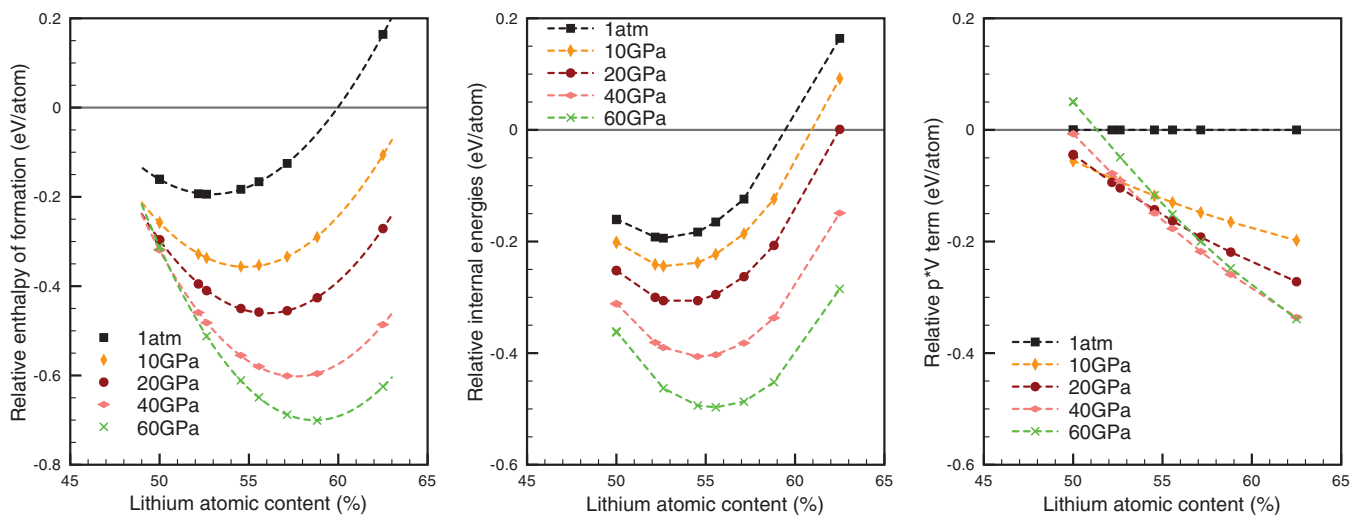

FIG. 6. (Color online) (Left) Ground-state enthalpies of formation for boron-deficient LiB_x structures, relative to the elements; (middle) relative internal energies for the same structures; (right) relative pV terms for the same structures. (Left) Dashed lines are quadratic fits to the enthalpies; (middle and right), lines are guide to the eye only.

VII. ANOTHER WAY TO MOVE OFF THE 1:1 STOICHIOMETRY: INTERCALATING LITHIUM LAYERS

One could also construct Li-B structures off the 1:1 stoichiometry in another way, by beginning with the metal sandwich structures and then progressively intercalating lithium layers between the individual "sandwich" layers. Structures of this type are actually found in group 1/group 13 binaries: the Li_5Ga_4 structure crystallizes in space group 164, *P-3m1*,[59] and Li_3Al_2 crystallizes in space group 166, *R-3m*.[60] In both structures, the Ga and Al atoms, respectively, form graphitic sheets (flat and buckled under pressure), separated by trigonal nets of Li. But in Li_5Ga_4 there is, compared to LiB, one additional lithium layer present per unit cell, so that the layer stacking is now —[-(LiGaLi)-Li-(LiGaLi)-]-. . . . When we try this geometry for Li_5B_4, we find this structure type to be on or close to the convex hull in the Li-B ground-state phase diagram over the entire pressure range examined. We did not perform a structure search for this phase, so we cannot comment on whether there are better structural alternatives for Li_5B_4.

As a side note, a very different structure for Li_5B_4 was reported in the experimental literature—with a short-range rhombohedral structure (space group *R3m*, Z = 1, a = 4.93 Å, $\alpha = 90°$), but with long-range disorder with body-centered cubic symmetry.[61,62] While this might have been an erroneous assignment of the hexagonal LiB structure, we find the short-range *R3m* structure to be very unstable indeed. It optimizes to a = 4.87 Å and $\alpha = 72.2°$, a huge deviation from the quasicubic experimental unit cell.

As with Li_5Ga_4, the Li_3Al_2 structure features graphitic Al sheets, separated by trigonal Li sheets. The actual stacking of the layers is —[-(LiAlLi)-Li-]-. . . to accommodate yet another lithium atom per unit cell, compared to the Li_5Ga_4 structure. The Li_3Al_2 structure type, when applied to Li_3B_2, is also found on or close to the convex hull for all pressures considered (again, no evolutionary structure search was performed for this stoichiometry). In Fig. 7, we show both the Li_5B_4 and Li_3B_2 structures. Note that the stacking of the lithium layers is (A)B(C)(A). . . for Li_5B_4 and (A)B(C)A(B)C(A). . . for Li_3B_2, where (. . .) now denotes a sandwich layer.

VIII. COMPARING BORON DEPLETED CHAINS AND INTERCALATED LITHIUM LAYERS

One could now imagine that manipulating the number of additional intercalated lithium layers (compared to pure LiB) would lead to a variety of stable stoichiometries between LiB and Li_3B_2, including Li_5B_4. This could then be yet a different explanation for the existence of stable LiB_x structures in the range $0.8 \leqslant x \leqslant 1$ than proposed in Ref. 37. We proceeded to construct in this manner the phases $Li_{11}B_{10}$, Li_8B_7, Li_7B_6, and Li_7B_5. In these structures, we adhered to the ABCA. . . lateral stacking for the lithium layers that was mentioned above, and with the appropriate alternate layering of simple lithium and boride sandwich layers to obtain the respective stoichiometries. Together with the already known LiB, Li_5B_4, and Li_3B_2 structures, we can sample the ground-state phases with lithium atomic content between 50% and 60%, in a similar way as has been done above for the boron chain structures.
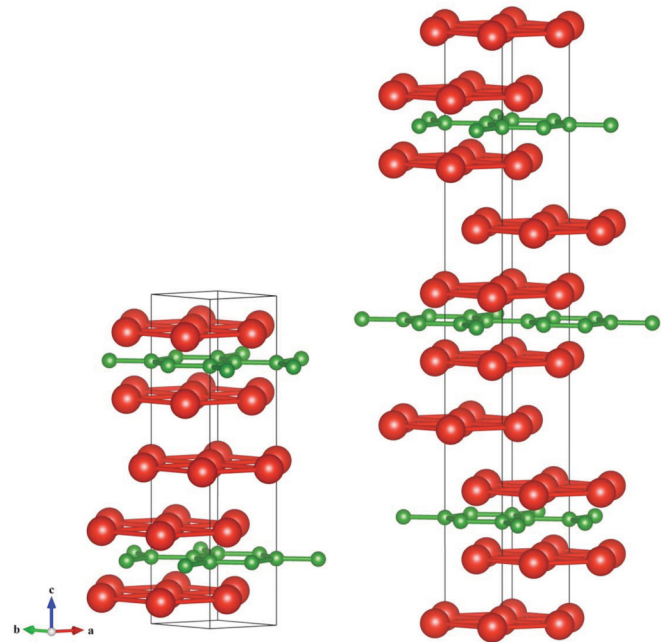

FIG. 7. (Color online) (Left) Ground-state Li_5B_4 phase in the Li_5Ga_4 structure, (right) the Li_3B_2 phase in the Li_3Al_2 structure. Both are shown at $P = 1$ atm.

Figure 8 shows the ground state enthalpies of formation of these layered structures as a function of stoichiometry and for various pressures. Increasing pressure always makes for more stable sandwich layer phases (compared to the elements). Going towards more lithium-rich layered phases increases the enthalpy of formation per atom, at all pressures. However, the most lithium-rich phase Li_3B_2 is at most 76 meV/atom removed from the convex hull (this is at $P = 10$ GPa), and is part of the convex hull for pressures $P \geqslant 50$ GPa. Because of the concave (or, at most, linear) dependence of the enthalpies on the lithium content, intermediate stoichiometries are found
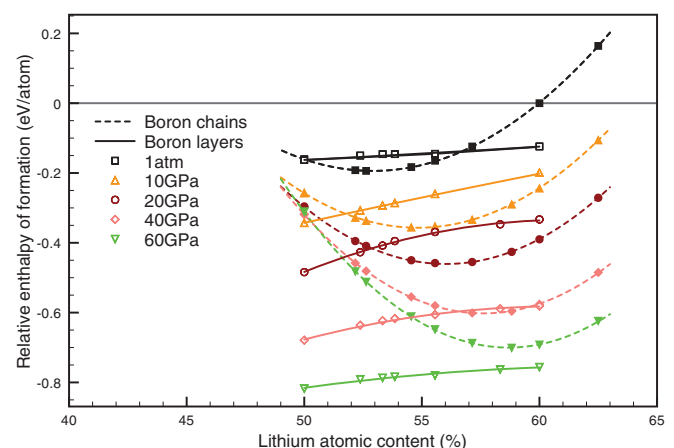

FIG. 8. (Color online) Ground-state enthalpies of formation for various boron chain structures (filled symbols, dashed lines) and sandwich structures (open symbols, solid lines), at various pressures. Dashed lines are quadratic fits (same as in Fig. 6), solid lines are cubic spline fits.

to be unstable with respect to decomposition into LiB and Li_3B_2 (the maximally intercalated structure).

At atmospheric pressure, boron chain structures, at their optimal composition around $LiB_{0.9}$, are clearly favored over the sandwich structure alternative. But we see from Fig. 8 *that the composition range where chain structures are more stable than sandwich structures reduces under pressure, and in fact vanishes above 40 GPa*: at atmospheric pressure, chain structures are more stable between 50% and 56.5% lithium content; at $P = 20$ GPa, between 52.8% and 61.3%; but at $P = 40$ GPa, only between 56.5% and 59.5%. However, absolute stability is measured with respect to possible escape routes, and even the most stable structure at a given stoichiometry might benefit from decomposition into other phases. Thus, by taking into account the other possible phases in the Li-B system (of which there are quite a few[16,17]), we can establish the range of absolute stability for the chain and sandwich structures; this will, of course, depend on pressure. Therefore even though chainlike structures are clearly not favored under pressure in the 1:1 stoichiometry (for example, as seen in Fig. 8, their enthalpy at $P = 60$ GPa is around 500 meV/atom higher than the layered *R-3m* structure), they might become stable with slightly increasing the relative concentration of lithium.

In Fig. 9, we show the results of this analysis: a finite range of stability of boron deficient LiB_x chain structures can be found up to pressures of $P \leqslant 35$ GPa. With increasing pressure, more boron-deficient structures are stable. At pressures higher than 35 GPa, the chain structures are not part of the convex hull in the Li-B phase diagram any more, and their decomposition into the 1:1-LiB sandwich structure (or, at $P \geqslant 70$ GPa: the NaTl structure) and more lithium-rich phases (we find a very stable Li_2B high-pressure phase we will report elsewhere[17]) is enthalpically favored.

We can also compare the structural properties of the various chains with experimental high-pressure room temperature data from Ref. 36. In Fig. 9, we plot both the c/a ratio and the c axis, both for the lithium sublattice, for various chain compositions (see also the SI for more details). Both of these quantities are very sensitive to the boron content in the system. We find very good agreement with the estimate in Ref. 36, that the initial sample composition at atmospheric pressure is $LiB_{0.92}$. The curious finding in experiment that above $P \geqslant 5$ GPa the c/a ratio *decreases* cannot be explained with a constant sample composition, however: for each chain structure, c/a increases monotonically as a function of pressure, irrespective of composition (this means, in accordance with arguments above, that the lithium sub-lattice in the ab plane is more easily compressed than the boron chains along c). From our calculations, we would instead argue that a decreasing c/a ratio corresponds to a loss in boron content under pressure (or additional uptake of excess lithium, possibly available in the pressure chamber). Specifically, we would estimate from the c/a ratios plotted in Fig. 9 that the boron content in LiB_x in the sample of Ref. 36 is about $0.75 \leqslant x \leqslant 0.80$ at $P = 40$ GPa. This is much lower than the initial boron content of $x = 0.92$, and in fact is in qualitative agreement with the stabilization of more boron-deficient structures under pressure.

Electronically, we find the lithium-rich sandwich structures to be metallic at all pressures. By way of example, we present here the properties of the known structure types, Li_5B_4 and
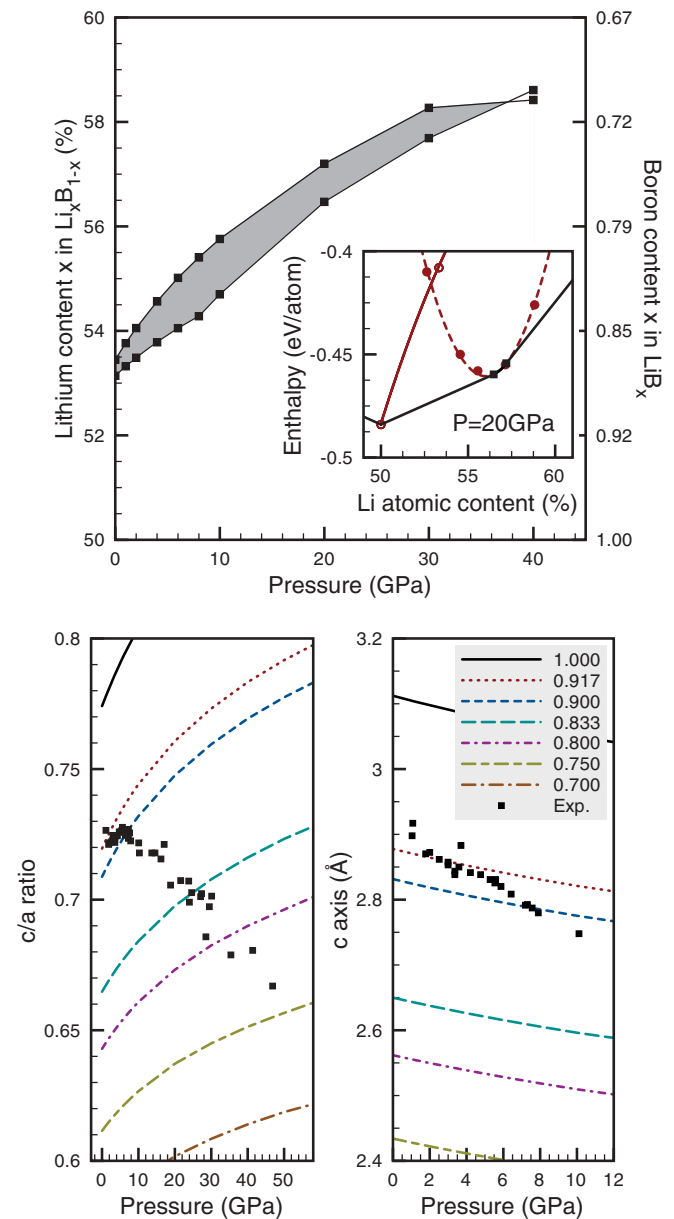

FIG. 9. (Color online) (Top) Stability range for ground-state boron chain structures as a function of pressure, indicated as the shaded area. The inset shows how the data points are acquired, here for the $P = 20$ GPa phase diagram: dashed and solid red lines are chain and sandwich enthalpy curves (see Fig. 8), solid black line is the convex hull, including part of the chain structure parabola. Two plots on the bottom compare the c/a ratio and c axis for various chain stoichiometries (labeled by x in LiB_x) with experimental results from Ref. 36.

Li_3B_2. The band structure and DOS of the *P-3m1* structure for Li_5B_4 confirm the two-dimensional character of the system, see Fig. 10. At $P = 1$atm, the boron layers are effectively decoupled, their bands degenerate, but at high pressures ($P = 80$ GPa shown in Fig. 10), they interact and the bands split. However, the boron layers are still substantially two-dimensional, as dispersion along the c axis is negligible.

The electronic structure of Li_3B_2 is very similar to Li_5B_4. The boron bands are near-degenerate at low pressures (see
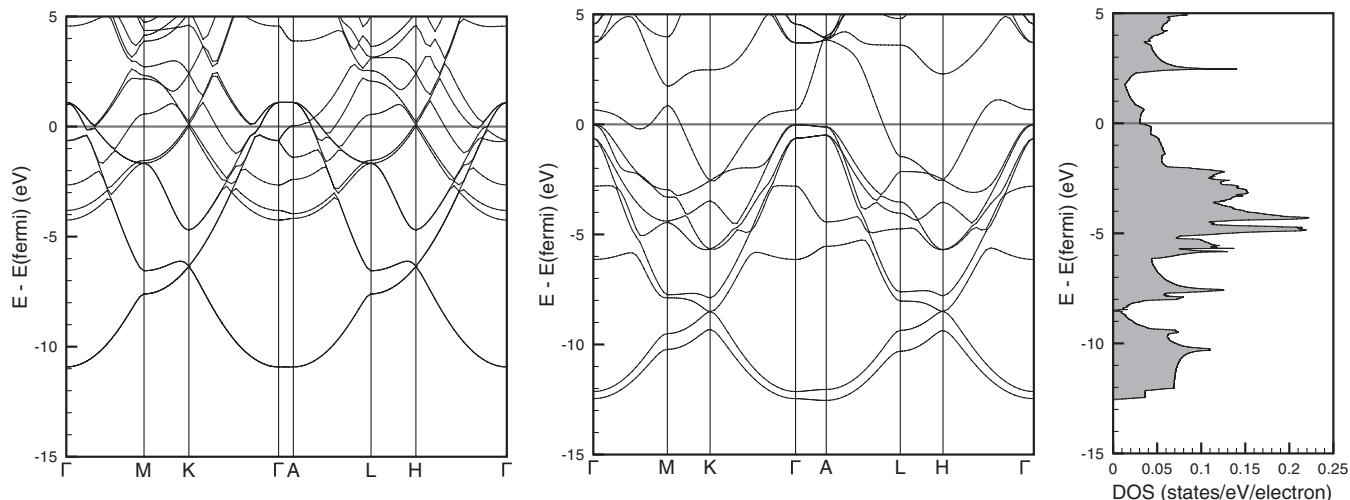
FIG. 10. Electronic band structure (left, $P = 1$ atm, and middle, $P = 80$ GPa) and DOS (right, $P = 80$ GPa) for the *P-3m1* ground-state structure of Li_5B_4.

Fig. 11) and distinctively two-dimensional. The DOS displays the two-dimensional character of the system, too. However, the Fermi energy under pressure falls into a wide pseudogap for both phases, the minimum of which (at $E = E_{Fermi} + 3.5$ eV for Li_3B_2, see Fig. 11) corresponds to a total valence electron count of about 30 electrons per unit cell (there are 27 valence electrons in the hexagonal unit cell of Li_3B_2); this in turn corresponds to the 1:1 stoichiometry LiB.

At atmospheric pressure, both the Li_5B_4 and Li_3B_2 structure are energetically competitive with LiB, see Fig. 12. There, we plot the enthalpies of formation of these structures with respect to the elements (solid lines in Fig. 12), and also, if they are not part of the convex hull, the enthalpy of the latter (dashed lines in Fig. 12). This is, for instance, the case at low pressures, where the chain-based structures are more stable in this composition range. The relative enthalpic order changes under moderate pressure ($P \geqslant 20$ GPa), where the *R-3m* structure of LiB is more stable than its more lithium-rich variants. And at $P \geqslant 60$ GPa, we do find that the layered structures are all

part of the convex hull in the phase diagram, and only at the highest pressures (when LiB assumes the NaTl structure) do they become unstable with respect to LiB and pure lithium. Note that all three phases experience a significant stabilization over the elements, in the case of LiB by more than 1.5eV per atom at $P = 300$ GPa.

IX. SUMMARY

We have presented results of a computational study on the high-pressure ground state properties of LiB and nearby boron-deficient phases. In agreement with experiment we show a stability region for compositions between 50 and 56.5% lithium, where boron chain depletion is preferred to lithium intercalation. That region narrows under pressure and above $P = 60$ GPa the strict 1:1 stoichiometry is favored, but in a very different NaTl structure. Consistently, the formation of "metal sandwiches" interspersed by pure lithium layers, produces stable metallic phases at low pressures. For LiB, the Zintl concept comes to the
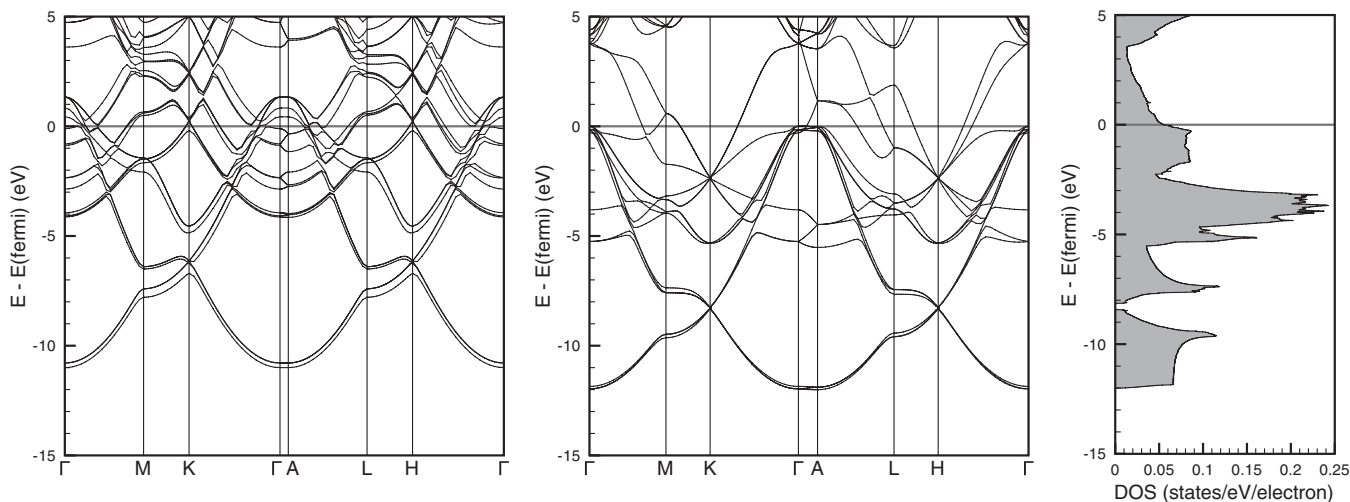

FIG. 11. Electronic band structure (left, $P = 1$ atm, and middle, $P = 80$ GPa) and DOS (right, $P = 80$ GPa) for the *R-3m* ground-state structure of Li_3B_2. The hexagonal unit cell was used for the band structures.
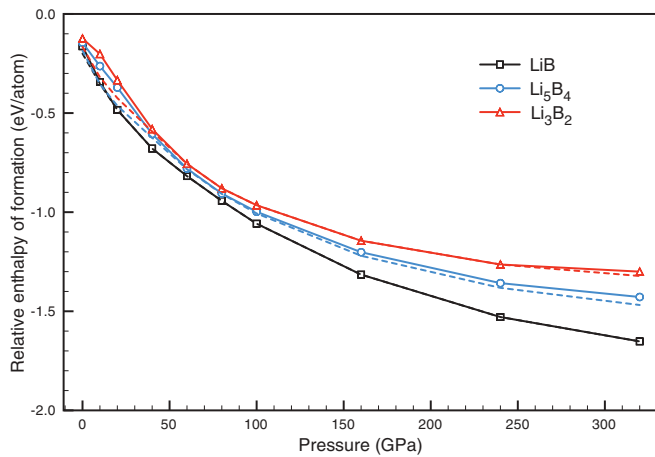
FIG. 12. (Color online) Ground-state enthalpies of formation for the LiB, Li_5B_4, and Li_3B_2 structures relative to the elemental crystals as a function of pressure. Dashed lines are the enthalpies of the convex hull for the respective stoichiometries, as obtained from our calculations.

fore in the high-pressure regime, where an insulating structure of the NaTl type is most stable. The special problem noted by others (B-B separations that are too short) of the on-stoichiometry chain structures of LiB is alleviated by stabilizing boron depletion. But one can also increase the relative Li:B ratio by intercalating lithium layers; this certainly happens for Li_3B_2. We analyze carefully the relative enthalpy of depleted chain and intercalated lithium layer alternatives as a function of

pressure; the composition range where chain structures are more stable narrows with pressure and vanishes above $P = 40$ GPa.

Lithium and boron are light elements, and dynamical effects could lead to changes in relative Gibbs free energies at finite temperatures. The fact that the experimental boundaries of the stability range of LiB_x are nearly independent of temperature for $T \leqslant 400°C$ could be interpreted that such effects are in fact not dominant.

*Corresponding author: ah736@cornell.edu

[1] Jian Lv, Yanchao Wang, Li Zhu, and Yanming Ma, Phys. Rev. Lett. **106**, 015503 (2011).

[2] Christophe L. Guillaume, Eugene Gregoryanz, Olga Degtyareva, Malcolm I. McMahon, Michael Hanfland, Shaun Evans, Malcolm Guthrie, Stanislav V. Sinogeikin, and H.-K. Mao, Nat. Phys. **7**, 211 (2011).

[3] M. Marqués, M. I. McMahon, E. Gregoryanz, M. Hanfland, C. L. Guillaume, C. J. Pickard, G. J. Ackland, and R. J. Nelmes, Phys. Rev. Lett. **106**, 095502 (2011).

[4] Takahiro Matsuoka and Katsuya Shimizu, Nature (London) **458**, 186 (2009).

[5] B. Rousseau, Y. Xie, Y. Ma, and A. Bergara, Eur. Phys. J. B **81**, 1 (2011).

[6] Norman Neil Greenwood and Alan Earnshaw, *Chemistry of the Elements* (Pergamon Press, New York, 1984).

[7] Barbara Albert and Harald Hillebrecht, Angew. Chem. Int. Ed. **48**, 8640 (2009).

[8] E. Yu. Zarechnaya, L. Dubrovinsky, N. Dubrovinskaia, Y. Filinchuk, D. Chernyshov, V. Dmitriev, N. Miyajima, A. El Goresy, H. F. Braun, S. Van Smaalen, I. Kantor, A. Kantor, V. Prakapenka, M. Hanfland, A. S. Mikhaylushkin, I. A. Abrikosov, and S. I. Simak, Phys. Rev. Lett. **102**, 185501 (2009).

[9] Artem R. Oganov, Jiuhua Chen, Carlo Gatti, Yanzhang Ma, Yanming Ma, Colin W. Glass, Zhenxian Liu, Tony Yu, Oleksandr Kurakevych, and Vladimir L. Solozhenko, Nature (London) **457**, 863 (2009).

[10] Georg Will and Klaus Ploog, Nature (London) **251**, 406 (1974).

[11] Georg Will and Bodo Kiefer, Z. Anorg. Allg. Chem. **627**, 2100 (2001).

[12] Donald E. Sands and J. L. Hoard, J. Am. Chem. Soc. **79**, 5582 (1957).

[13] R. E. Hughes, C. H. L. Kennard, D. B. Sullenger, H. A. Weakliem, D. E. Sands, and J. L. Hoard, J. Am. Chem. Soc. **85**, 361 (1963).

[14] V. V. Brazhkin, T. Taniguichi, M. Akaishi, and S. V. Popova, J. Mater. Res. **19**, 1643 (2004).

[15] P. Villars, H. Okamoto, and K. Cenzual, *ASM Alloy Phase Diagrams Center* (ASM International, Materials Park, OH, 2006).

[16] H. B. Borgstedt and C. Guminski, J. Phase Equilib. **24**, 572 (2003).

[17] Andreas Hermann, Alexandra McSorley, N. W. Ashcroft, and Roald Hoffmann (to be published).

[18] Bernd Hartke, J. Phys. Chem. **97**, 9973 (1993).

[19] Artem R. Oganov, Andriy O. Lyakhov, and Mario Valle, Acc. Chem. Res. **44**, 227 (2011).

[20] David C. Lonie and Eva Zurek, Comput. Phys. Commun. **182**, 372 (2011).

[21] James Kennedy and Russell Eberhart, in *Proceedings IEEE International Conference On Neural Networks, 1995* (IEEE, Perth, WA, 1995), pp. 1942–1948.

[22] Yanchao Wang, Jian Lv, Li Zhu, and Yanming Ma, Phys. Rev. B **82**, 094116 (2010).

[23] Peter Hohenberg and Walter Kohn, Phys. Rev. **136**, B864 (1964).

[24] Walter Kohn and L. J. Sham, Phys. Rev. **140**, A1133 (1965).

[25] G. Kresse and J. Furthmüller, Phys. Rev. B **54**, 11169 (1996).

[26] P. E. Blöchl, Phys. Rev. B **50**, 17953 (1994).

[27] G. Kresse and D. Joubert, Phys. Rev. B **59**, 1758 (1999).

[28] John P. Perdew, Kieron Burke, and Matthias Ernzerhof, Phys. Rev. Lett. **77**, 3865 (1996).

[29] Hendrik J. Monkhorst and James D. Pack, Phys. Rev. B **13**, 5188 (1976).

[30] See Supplemental Material at http://link.aps.org/supplemental/10.1103/PhysRevB.86.144110 for crystal structures, equation of state fits, and pressure dependencies of structural and electronic properties.

[31] Francis Birch, Phys. Rev. **71**, 809 (1947).

[32] Zhijian Liu, Xuanhui Qu, Baiyun Huang, and Zhiyou Li, J. Alloys Compd. **311**, 256 (2000).

[33] Michael Wörle and Reinhard Nesper, Angew. Chem. Int. Ed. **39**, 2349 (2000).

[34] H. Rosner and W. E. Pickett, Phys. Rev. B **67**, 054104 (2003).

[35] Michael Wörle, Reinhard Nesper, and Tapan K. Chatterji, Z. Anorg. Allg. Chem. **632**, 1737 (2006).

[36] A. Lazicki, Russell J. Hemley, W. E. Pickett, and Choong-Shik Yoo, Phys. Rev. B **82**, 180102 (2010).

[37] Aleksey N. Kolmogorov and Stefano Curtarolo, Phys. Rev. B **74**, 224507 (2006).

[38] V. I. Kasatochkin, A. M. Sladkov, Y. P. Kudryavtsev, N. M. Popov, and V. V. Korshak, Dokl. Chem. **177**, 1031 (1967).

[39] P. P. K. Smith and Peter R. Buseck, Science **216**, 984 (1982).

[40] A. Greenville Whittaker, Science **200**, 763 (1978).

[41] Holger Braunschweig, Rian D. Dewhurst, Kai Hammond, Jan Mies, Krzysztof Radacki, and Alfredo Vargas, Science **336**, 1420 (2012).

[42] John P. Perdew, J. A. Chevary, S. H. Vosko, Koblar A. Jackson, Mark R. Pederson, D. J. Singh, and Carlos Fiolhais, Phys. Rev. B **46**, 6671 (1992).

[43] Jochen Heyd, Gustavo E. Scuseria, and Matthias Ernzerhof, J. Chem. Phys. **118**, 8207 (2003).

[44] Jochen Heyd, Gustavo E. Scuseria, and Matthias Ernzerhof, J. Chem. Phys. **124**, 219906 (2006).

[45] Stefan Grimme, J. Comput. Chem. **27**, 1787 (2006).

[46] Aleksey N. Kolmogorov and Stefano Curtarolo, Phys. Rev. B **73**, 180501 (2006).

[47] Matteo Calandra, Aleksey N. Kolmogorov, and Stefano Curtarolo, Phys. Rev. B **75**, 144506 (2007).

[48] K. Kishio and J. O. Brittain, J. Phys. Chem. Solids **40**, 933 (1979).

[49] W. Baden, P. C. Schmidt, and Alarich Weiss, Phys. Status Solidi A **51**, 183 (1979).

[50] E. Zintl, Angew. Chem. **52**, 1 (1939).

[51] Reinhard Nesper, Prog. Solid State Chem. **20**, 1 (1990).

[52] Hans-Jürgen Meyer, in *Moderne Anorganische Chemie*, edited by Erwin Riedel (Walter de Gruyter, Berlin, 1998), pp. 329–528.

[53] E. Zintl and W. Dullenkopf, Z. Phys. Chem. B **16**, 195 (1932).

[54] F. P. Bundy, H. P. Bovenkerk, H. M. Strong, and R. H. Wentorf, J. Chem. Phys. **35**, 383 (1961).

[55] Bruno Rousseau and N. W. Ashcroft, Phys. Rev. Lett. **101**, 046407 (2008).

[56] J. B. Neaton and N. W. Ashcroft, Phys. Rev. Lett. **86**, 2830 (2001).

[57] J. B. Neaton and N. W. Ashcroft, Nature **400**, 141 (1999).

[58] J. S. Schilling, in *Handbook of High-Temperature Superconductivity: Theory and Experiment*, edited by John Robert Schrieffer and James S. Brooks (Springer, Hamburg, 2007), pp. 427–462.

[59] Joachim Stöhr and Herbert Schäfer, Z. Anorg. Allg. Chem. **474**, 221 (1981).

[60] Karl-Friedrich Tebbe, Hans Georg Von Schnering, Barbara Rüter, and Gisela Rabeneck, Z. Naturforsch. B **28**, 600 (1973).

[61] F. E. Wang, M. A. Mitchell, R. A. Sutula, J. R. Holden, and L. H. Bennett, J. Less-Common Met. **61**, 237 (1978).

[62] Frederick E. Wang, Metall. Mater. Trans. A **10**, 343 (1979).